

Computing with carbon nanotubes: Optimization of threshold logic gates using disordered nanotube/polymer composites

M. K. Massey, A. Kotsialos, F. Qaiser, D. A. Zeze, C. Pearson, D. Volpati, L. Bowen, and M. C. Petty

Citation: *Journal of Applied Physics* **117**, 134903 (2015); doi: 10.1063/1.4915343

View online: <http://dx.doi.org/10.1063/1.4915343>

View Table of Contents: <http://scitation.aip.org/content/aip/journal/jap/117/13?ver=pdfcov>

Published by the **AIP Publishing**

Articles you may be interested in

[Enhancement of ambipolar characteristics in single-walled carbon nanotubes using C60 and fabrication of logic gates](#)

Appl. Phys. Lett. **106**, 103501 (2015); 10.1063/1.4914476

[Controllable terahertz conductivity in single walled carbon nanotube/polymer composites](#)

J. Appl. Phys. **117**, 023115 (2015); 10.1063/1.4905958

[A simulation study on the combined effects of nanotube shape and shear flow on the electrical percolation thresholds of carbon nanotube/polymer composites](#)

J. Appl. Phys. **109**, 084342 (2011); 10.1063/1.3573668

[Homogeneous carbon nanotube/polymer composites for electrical applications](#)

Appl. Phys. Lett. **83**, 2928 (2003); 10.1063/1.1616976

[Electrical properties of singlewalled carbon nanotubes-PMMA composites](#)

AIP Conf. Proc. **544**, 363 (2000); 10.1063/1.1342534

You don't still use this cell phone

or this computer

Why are you still using an AFM designed in the 80's?

It is time to upgrade your AFM

Minimum \$20,000 trade-in discount for purchases before August 31st

Asylum Research is today's technology leader in AFM

dropmyoldAFM@oxinst.com

OXFORD INSTRUMENTS
The Business of Science®

Computing with carbon nanotubes: Optimization of threshold logic gates using disordered nanotube/polymer composites

M. K. Massey,¹ A. Kotsialos,¹ F. Qaiser,¹ D. A. Zeze,¹ C. Pearson,¹ D. Volpati,^{1,2} L. Bowen,³ and M. C. Petty¹

¹Centre for Molecular and Nanoscale Electronics, School of Engineering and Computing Sciences, Durham University, DH1 3LE, Durham, United Kingdom

²São Carlos Institute of Physics, University of São Paulo-USP, PO Box 369, 13566-590 São Carlos, SP, Brazil

³Department of Physics, Durham University, DH1 3LE Durham, United Kingdom

(Received 19 December 2014; accepted 7 March 2015; published online 7 April 2015)

This paper explores the use of single-walled carbon nanotube (SWCNT)/poly(butyl methacrylate) composites as a material for use in unconventional computing. The mechanical and electrical properties of the materials are investigated. The resulting data reveal a correlation between the SWCNT concentration/viscosity/conductivity and the computational capability of the composite. The viscosity increases significantly with the addition of SWCNTs to the polymer, mechanically reinforcing the host material and changing the electrical properties of the composite. The electrical conduction is found to depend strongly on the nanotube concentration; Poole-Frenkel conduction appears to dominate the conductivity at very low concentrations (0.11% by weight). The viscosity and conductivity both show a threshold point around 1% SWCNT concentration; this value is shown to be related to the computational performance of the material. A simple optimization of threshold logic gates shows that satisfactory computation is only achieved above a SWCNT concentration of 1%. In addition, there is some evidence that further above this threshold the computational efficiency begins to decrease. © 2015 AIP Publishing LLC.

[<http://dx.doi.org/10.1063/1.4915343>]

I. INTRODUCTION

The topic of unconventional computing is attracting increasing attention, particularly as it is thought that the miniaturization limits of conventional electronics could soon be reached. Alternatives to MOSFET technology based on single crystal silicon are being sought. An important stream of unconventional computing research is based on the concept of evolvable hardware. In this approach, an evolutionary algorithm is applied directly to a piece of material mounted on a suitably designed hardware platform. A pre-selected physical property is then “evolved,” bringing the material to a state where it is able to perform meaningful computation. This methodology has become known as *evolution in material*.¹ It is in this area of study that the materials described here are of particular interest.²

The experimental set-up for this evolution process is illustrated in Figure 1. The diagrams to the left illustrate how the material operates as a “black box” computational device. A range of incident signals result in a response from the material and the recorded output data are interpreted as a computation based on a pre-specified scheme. There are two categories of incident signals: the data input, which are used as arguments in the computational task; and the computer generated configuration input signals, which evolve and bring the material to the desired computation-inducing state. The latter are selected by an evolutionary algorithm, which can be regarded more generally as an optimization search algorithm. The evolution is performed by following an iterative scheme searching the space of possible configuration inputs. A set of argument inputs for

which the corresponding outputs are known (based on the computation interpretive scheme adopted) is used repetitively in the optimization search loop. Convergence is achieved when the computation task for the selected arguments is performed correctly by the material. The bottom left diagram in Figure 1 depicts a sketch of the random material structure and shows how the inputs are applied and the corresponding output measurements collected. Note that the signals are applied to the material at known fixed locations. However, the material itself has a randomly dispersed unknown electrical structure.

The top-right image in Figure 1 shows the half-adder circuit with its truth table given below. In previous work³ we have shown that the evolutionary approach can be applied to a single-walled carbon nanotube/polymer composite. One of the computation tasks selected was to configure the material’s conductance so that the Boolean function of the half-adder could be calculated for all possible binary inputs. This work explores in more detail the role that the material plays during the optimization process.

II. MATERIALS, EXPERIMENTAL APPROACH, AND PROBLEM FORMULATION

A. Materials

Thin films of single-walled carbon nanotubes (SWCNTs) embedded within poly(butyl-methacrylate) (PBMA) were used in this work. The formulations were created following similar methods of material preparation of PMMA/SWCNT composites.⁴⁻⁶ The composites were made by adding

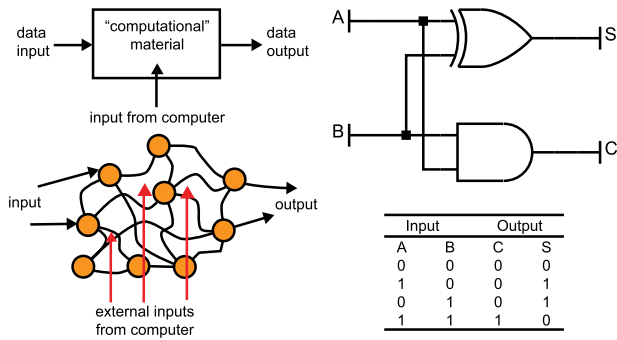


FIG. 1. Black box and concept diagrams behind “evolution in-materialio” (left). Block diagram and truth table for a half adder: A,B = inputs, C = carry, S = sum.

SWCNTs (Carbon Nanotechnologies Inc. Houston, TX, USA) to PBMA powder (Sigma Aldrich, M_w 337 000). These powders were then dispersed in anisole (VWR, analytical reagent grade), with the aid of an ultrasonic probe (Cole-Palmer 750W ultrasonic homogenizer) at a power of 20%. The dispersions were visually uniform and stable over a long period with no obvious precipitation of the SWCNTs from suspension. A range of nanotube concentrations was used with a fixed polymer concentration to allow comparison of the conductivities of different samples. This material system was chosen as a convenient electrically conductive network, the properties of which can be easily changed by modifying the nanotube concentration. Polymer/SWCNT mixtures form electrically complex films due to the dielectric properties of the PBMA, mixed with differing electronic properties of SWCNTs (both metallic and semiconducting).

Viscosity measurements were made on the composites in liquid form using a TA instruments AR 2000ex rheometer; a 40 mm diameter parallel plate geometry was used for all measurements.

B. Thin film formation

Thin films of SWCNT/PBMA were deposited on glass substrates with patterned electrode arrays, which were fabricated using conventional etch-back photo-lithographic techniques from chromium/gold on standard borosilicate glass slides. Two 4×4 grid arrays were prepared on each slide; the contact pads for the electrodes had a diameter of $50 \mu\text{m}$ and a pitch of $100 \mu\text{m}$.

The films were deposited by spin coating, with a final spin speed of 5000 rpm, and then dried on a hotplate at 85°C for 10 min. The film thickness was dependent on the nanotube concentration and was approximately $1\text{--}5 \mu\text{m}$. A scanning electron microscope image of a typical region of one of these composite films is shown in Figure 2. It can be seen that the nanotubes, although present in bundles, are well dispersed within the polymer.

Electrical measurements were performed on the spin-coated films in air using a Keithley 2635A sourcemeter with a custom designed MATLAB interface program. Scanning electron microscope (SEM) images were captured with an FEI Helios Nanolab 600 microscope.

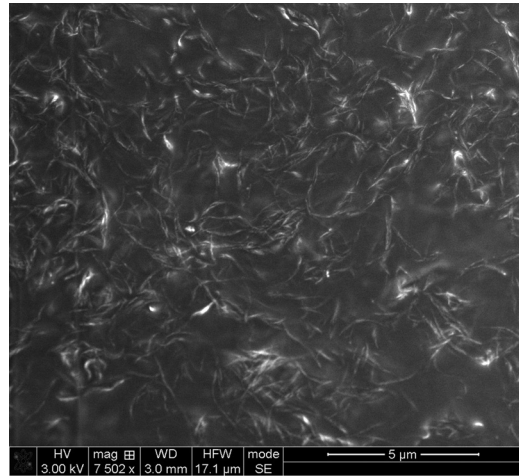


FIG. 2. Scanning electron microscope image of a typical region of a spin coated SWCNT/PBMA composite (SWCNT concentration of 2.39 wt. %).

C. Hardware platform

It was necessary to apply and monitor many signals (up to 16 channels) on one sample for this work. The complete set-up of the hardware platform consisted of a desktop computer (PC) to run the optimization algorithms, a signal generation device and the computational device (CD), consisting of the microelectrode array and the composite SWCNT/PBMA thin film, Figure 3. The signal generation device was driven by a micro-controller handling the serial communication to the PC and controlling the various analogue-to-digital and digital-to-analogue converters (ADC/DAC) required to apply and record voltage signals. All of the inputs and outputs to the ADCs/DACs were buffered to isolate the electronics from the material. A schematic diagram of a system with two inputs, five configuration voltages and two outputs, is provided in Figure 4.

D. Computing problem formulation

To configure the material’s conductance in order to compute the OR, AND and half-adder Boolean functions an optimization problem is formulated and solved iteratively, with the objective function J being evaluated directly from the material, i.e., an optimization with hardware-in-the-loop is performed. The scheme used for interpreting the measurements collected from the material is based on a fixed number of voltage thresholds for each of the two outputs of the half-

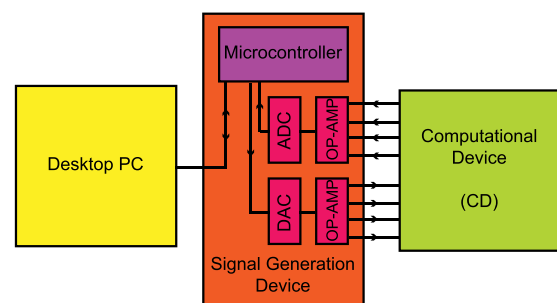


FIG. 3. Block diagram showing the hardware used to perform computation experiments.

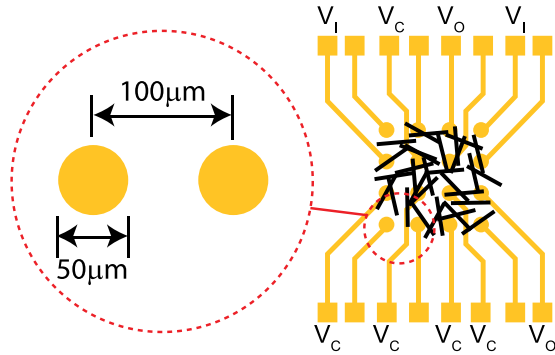


FIG. 4. Example system with two inputs, two outputs and five configuration nodes. A detail view of the electrode dimensions is also given.

adder. For the carry, a single threshold $\theta_{1,1}$ is used; a measured output larger than $\theta_{1,1}$ is interpreted as logical 1, otherwise as 0. Two threshold voltages are used for the output measurements corresponding to the sum, $\theta_{2,1}$ and $\theta_{2,2}$; a voltage measured within the band $[\theta_{2,1}, \theta_{2,2}]$ is considered as a logical 1, otherwise any voltage measurement outside this interval is interpreted as a logical 0. This interpretation scheme of the measured outputs is followed consistently for the evaluations of the objective function during the optimization algorithm's iterations.

The general optimization problem formulation is as follows. The problem parameters are the number of binary inputs n (two for all cases considered here), the number of configuration voltages r ; the number of binary outputs m (one for the OR and AND gates and two for the half-adder); the number of thresholds L_j used for measurements at output $j = 1, \dots, m$ (one for the carry and two for the sum); the lower and upper bounds of the voltages applied at the electrodes, V_{\min} and V_{\max} , respectively; the truth table of the desired logical circuit $\mathbf{Y}(\mathbf{A}) \in \{0, 1\}^m$ (shown in Figure 1 for the half-adder), where $\mathbf{A} = [A_1 \dots A_n]^T \in \{0, 1\}^n$ is the binary input vector; the number of examples K used for training the material; and the upper bound of a scaling factor β , B_{\max} .

The decision variables are the voltage levels V_{b_1} and V_{b_0} which signify a logical 1 or 0, respectively, at the input electrodes (typically $V_{b_0} = 0$ V); the configuration voltages V_{q_i} , $q = 1, \dots, r$ used for affecting the measurements at the material's output locations; and the scaling factor $\beta \in [0, B_{\max}]$, without units, used for calculating threshold values. Hence, a candidate solution is a vector of the form

$$\mathbf{x} = [V_{b_0} V_{b_1} V_1 \dots V_r \beta]^T. \quad (1)$$

Training examples are randomly pre-selected and given as inputs. A training example with index $k = 1, \dots, K$ is a pair of the form $(\mathbf{A}^{(k)}, \mathbf{Y}(\mathbf{A}^{(k)}))$. The condition $K > 2^n$ must hold in order to get a sufficient number of training examples representing equally each possible input in the formed objective function.

The objective function J selected is a quadratic expression of the error when a potential solution \mathbf{x} is applied to the material and the collected measurements are interpreted according to the previously described threshold logic scheme F_j for each output location j . The measurement at j ,

$M_j^{(k)}(\mathbf{x}, \mathbf{A}^{(k)})$, is the measured voltage when binary inputs $\mathbf{A}^{(k)}$ are applied and $H_j(\mathbf{x}, \mathbf{A}^{(k)})$ is the corresponding binary outcome when F_j is used. The individual contribution of training example k to the objective function, i.e., the total square error, is $\sum_{j=1}^m [H_j(\mathbf{x}, \mathbf{A}^{(k)}) - Y_j(\mathbf{A}^{(k)})]^2$. Hence, the optimization problem at hand is

$$\min_{\mathbf{x}} J = \sum_{k=1}^K \sum_{j=1}^m [H_j(\mathbf{x}, \mathbf{A}^{(k)}) - Y_j(\mathbf{A}^{(k)})]^2 \quad (2)$$

subject to

$$\mathbf{b}_\ell \leq \mathbf{x} \leq \mathbf{b}_u, \quad (3)$$

$$\theta_{j,p}(\mathbf{x}) = f_{j,p}(\mathbf{x}), j = 1, \dots, m, p = 1, \dots, L_j \quad (4)$$

$$H_j(\mathbf{x}, \mathbf{A}^{(k)}) = F_j[M_j(\mathbf{x}, \mathbf{A}^{(k)}), \theta_j(\mathbf{x})] \in \{0, 1\} \\ j = 1, \dots, m, \quad (5)$$

where $\mathbf{b}_\ell = [V_{\min}, \dots, V_{\min}, B_{\min}]^T$, $\mathbf{b}_u = [V_{\max}, \dots, V_{\max}, B_{\max}]^T$, and $f_{j,p}(\mathbf{x})$ is a pre-specified functional dependency of the threshold voltages to the decision variables.³ Note there are no ordering constraints for the thresholds θ_j . The algorithms used converge to a solution where this ordering holds true.

In view of the binary nature of the optimization problem where partial derivatives are not defined uniquely, classical-gradient based methods are not appropriate. Instead, population based optimization methods are more suitable. The important aspect of the implementation here, is the fact that the problem's objective function (2) is calculated directly on the hardware as a response to the combined 0–1 pulses of size V_{b_0} and V_{b_1} , respectively, and incident configuration voltages V_1, \dots, V_r . For calculating the objective function's value at a point \mathbf{x} , the following procedure is followed: first, the configuration voltages of \mathbf{x} are applied; these are kept fixed as a random sequence of K pairs of voltages $(V_{b_0}^{(k)}, V_{b_1}^{(k)})$, $k = 1, \dots, K$, representing logical pairs of 0s and 1s, are applied at the two input electrodes; for every such input pair k a voltage measurement is collected from the output electrodes. The result is the collection of K responses at the end of the random input sequence. Since \mathbf{x} includes a β , specific thresholds are determined in view of Eq. (4); using these, the K output measurements are interpreted as a logical 0 or 1 according to (5). Summing up and squaring the discrepancies between the known result corresponding to the logic interpretation of $(V_{b_0}^{(k)}, V_{b_1}^{(k)})$ and the application of (5) to the output measurements, before sending any new possible solution for evaluation at the board, gives the value of objective function (2). It is this value that is communicated back to the algorithm working in the PC.

The algorithm terminates when a zero value of J is observed for a particular solution \mathbf{x}^* or when the maximum numbers of iterations allowed is reached. At this point, zero voltages are applied at all electrodes. Subsequently, \mathbf{x}^* is sent back to the board and the optimal configuration voltages are applied and the electrodes are kept charged. An arbitrary

sequence of binary pairs is generated (different than the one used for finding \mathbf{x}^*) which are used as successive inputs. Again, the material's responses are collected, while $V_1 \dots V_r^*$ are applied, and are interpreted using the resulting optimal thresholds. This is the verification phase, where the optimal solution is tested on new binary input sequences. It turns out that an optimal solution \mathbf{x}^* that gives $J(\mathbf{x}^*) = 0$ retains this property for the verification input data as well.

The well-known Nelder-Mead (NM) algorithm⁷ with random periodic restart, as suggested in Ref. 8 was used for solving problem (2)–(5) due to its simplicity of implementation. The NM algorithm uses a simplex of $(r + 3) + 1$ (or in the case $V_{b_0} := 0$, $(r + 2) + 1$) points and requires the evaluation of the objective function for each of them. By applying at each iteration a reflection, expansion, contraction or reduction operation on the simplex, it gradually converges to a minimum, which in the case of Boolean circuits has to be zero. All these operations are performed on the PC, whereas the evaluation of (2) is performed on the board.

The NM algorithm, as such, is quite a simple but extensively tested and used method for function minimization. More efficient and sophisticated population-based algorithms, evolution inspired or not, can be used. However, the NM is sufficient for the purposes of this paper, as it is able to perform satisfactorily and consistently. An investigation regarding the suitability and performance of genetic algorithms and swarm intelligence methods will be reported elsewhere.

III. RESULTS AND DISCUSSION

A. Morphological and electrical characterisation

1. Viscosity

The shear stress τ in a material is related to the shear rate γ and its viscosity η , according to

$$\tau = \eta\gamma. \quad (6)$$

A linear relationship between shear rate and stress is assumed. In general, polymer blends of SWCNTs do not obey this simple relationship.⁹ Figure 5 shows shear rate

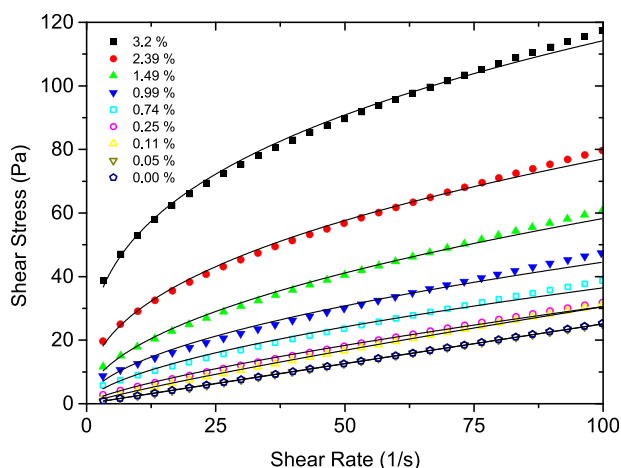


FIG. 5. Shear stress versus shear rate for various SWCNT/PBMA composites of varying SWCNT concentration.

versus shear stress data (symbols) for a range of different SWCNT concentrations (expressed as a fraction of the polymer weight). The polymer/SWCNT blend shows typical behavior associated with non-Newtonian liquids undergoing shear thinning, above all but the lowest concentrations, where the viscosity of the material reduces with higher rates of shear.

As the dependence of strain upon stress is clearly non-linear additional parameters are needed to fit the experimental data. A common power law used to describe shear-thinning is

$$\tau = A_C \gamma^n, \quad (7)$$

where the parameters to be fitted are the consistency A_C and the power law index n . Newtonian behavior is observed when $n = 1$, i.e., when shear stress is proportional to shear rate. The solid lines plotted in Figure 5 have been obtained using Eq. (7), and show reasonable (within experimental error) fits to the experimental data points. The parameters extracted from this fitting are given in Table I. For the pure polymer, the viscosity is 0.3 Pa.s and the power law index is 1, indicating Newtonian behavior. When a very small percentage of SWCNTs is added to the polymer (0.05%) the viscosity and power law index remain the same, showing that the SWCNTs have minimal, if any, effect on the polymer matrix. However, above 0.11% the A_C value starts increasing rapidly, and the value of n decreases, showing typical values for a material undergoing shear-thinning. This decrease in apparent viscosity (shear-thinning) could be attributed to the weak bonds between the SWCNT ropes being broken by the shear force. This would explain the much higher viscosity at low rates of shear; the smaller force is unable to break up the bundles of SWCNTs. This change is important as not only does it affect the thickness of the spin-coated films, but also helps to explain the change in electrical conductivity noted within the material.

Figure 6 shows how the apparent viscosity varies with SWCNT concentration (using the same data as that presented in Table I). The graph shows two distinct regions with differing gradients. The first region, (up to 1%) shows a steep gradient where the viscosity is increasing rapidly with an increase in SWCNT solid in the polymer mixture. Above this point (1% nanotube concentration), the log of viscosity continues to increase linearly, but with a much reduced

TABLE I. Consistency and power law index values for the curve fit to experimental data in Figure 5.

Concentration (wt. %)	A_C (Pa.s)	n
3.20	24.9	0.33
2.39	11.2	0.42
1.49	5.8	0.50
0.99	3.8	0.53
0.74	2.4	0.59
0.25	1.0	0.74
0.11	0.58	0.86
0.05	0.3	1.00
0.00	0.3	0.99

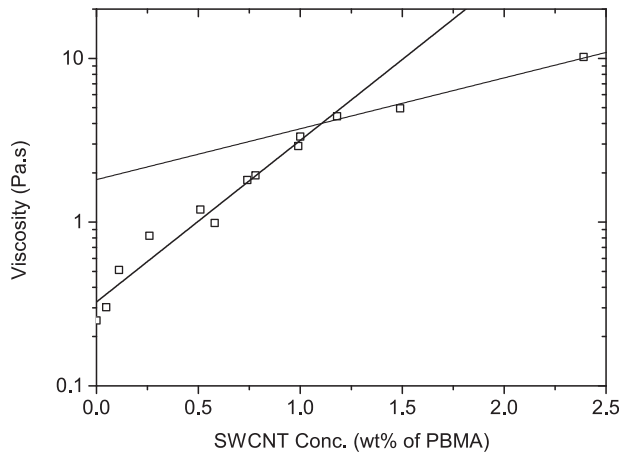


FIG. 6. Viscosity versus concentration for SWCNT/PBMA composites, with linear lines of best fit to the data.

gradient. It is likely in the first region, larger and larger bundles/meshes of SWCNTs are forming within the polymer, quickly increasing the viscosity. Above 1% SWCNT concentration, an interconnected mesh of SWCNTs is already present throughout the polymer, so any additional SWCNT content only has a minimal impact on the viscosity.

2. Electrical

Current versus voltage (I - V) measurements were made using adjacent electrodes with a separation of 50 μm . The conductivity increased with an increase in SWCNT concentration and the relationship between current and voltage was non-linear for all nanotube concentrations tested. The current measured at the lowest concentration of 0.11% was in the nA range. This increased by many orders of magnitude up to mA for the highest concentration of 2.39%. The increase in conductivity may be linked to the formation of interconnected SWCNT bundles within the composite, in a manner similar to the increase in viscosity noted in Sec. III A 1.

Figure 7 reveals how the current through the material varies with the concentration at a fixed bias of 10 V. The log of current increases linearly with increasing SWCNT concentration up to 1% and then increases linearly at a different

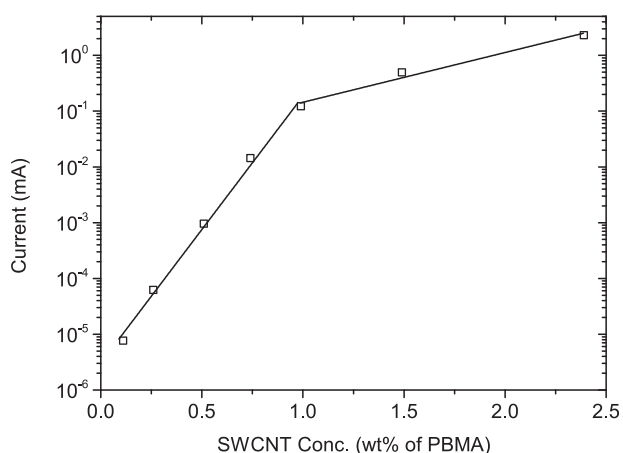


FIG. 7. Current versus concentration at a fixed bias of 10 V for SWCNT/PBMA composites, with linear lines of best fit to the data.

(reduced) gradient. The 1% SWCNT concentration is thought to be the electrical percolation threshold of the network; above this is a region of relatively high conductivity, which is less affected by the increase in SWCNT concentration as an interconnected network is already present. There are several reports in the literature for unmodified SWCNT/PMMA composites with percolation thresholds between 0.17 and 0.70%.^{6,10} The polymer, SWCNT source and any additional purification and/or functionalization of the SWCNTs can greatly affect the percolation threshold. Our data are consistent with the literature, indicating a percolation threshold in the range reported by others.⁵ It should be noted that no direct comparison can be made as the polymer used has a different chain length (butyl instead of methyl groups) which will affect the interaction between the SWCNTs and polymer. Our experience has suggested that the longer chain length (a more hydrophobic polymer) appears to aid in suspension forming with our PBMA based materials showing greater stability than PMMA alternatives.

The logarithms of the current versus voltage data were plotted to attempt to understand the conduction mechanisms at work within the film. The high concentration material showed that current was directly proportional to voltage with a slope of 1, indicating Ohmic conduction. However, the sign of temperature versus resistance measurements rule out metallic conduction. The lower concentration material had a slope of 1.5, suggesting that other mechanisms were at work within the network. Space charge limited conduction (SCLC) is reported for similar networks,¹¹ resulting in a quadratic relationship between voltage and current. This is probably not the case in this work. The Poole-Frenkel (PF) effect is a bulk trap-regulated process operating at high electric fields ($>10^6$ V/m) and has been widely reported as a possible mechanism for conduction in carbon nanotube networks.^{12,13} The current versus voltage dependence can be written as

$$I \propto V \exp\left(-\frac{E_d - \beta_{PF} V^{1/2}}{kT}\right), \quad (8)$$

where β_{PF} is the Poole-Frenkel constant given by

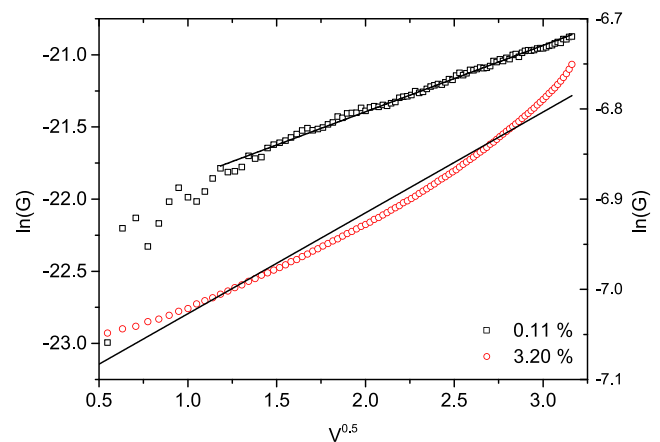


FIG. 8. Poole-Frenkel fit at low (0.11%) and high (3.20%) nanotube concentrations. Best fit lines of $y = a + bx$ plotted to reveal a gradient of 0.46 for the lowest concentration, the higher concentration does not show a linear relationship between I and V .

$$\beta_{PF} = \left(\frac{e^3}{\pi \epsilon_0 \epsilon_r d} \right)^{\frac{1}{2}}. \quad (9)$$

Figure 8 shows a plot of $\ln(I/V)$ versus $V^{0.5}$ for the same two extremes of SWCNT concentration previously analyzed. If the low field values are ignored (below 1 V) then a linear response is observed for the low concentration with a gradient of 0.46. This gives a relative permittivity value of about unity. Given the various approximations used in developing the simple PF model, this result is consistent with the PF process operating in our low nanotube concentration films.^{12,13}

However, throughout the range of data there is no linear fit for the higher SWCNT concentration samples, suggesting that Poole-Frenkel is not the dominant mechanism at work in these films.

B. Material optimization for computation

It was shown in the previous subsection that the SWCNT/PBMA composites possess a complex electrical structure, with a field dependent conductivity if the concentration is below a certain threshold. Using this knowledge, computer controlled optimization of logic circuits was performed using the equipment described in Sec. II.

There are two parameters to be discussed for rating the quality of a given material: the number of iterations to converge to an optimal solution and the objective function value of the optimal solution. This value states how successful the solution reached is at approximating a circuit's Boolean function, with a value of 0 signifying perfect behavior. The number of iterations it takes the specific implementation of the NM algorithm to converge to a solution provides a sense of how well the material's properties used for computation can be manipulated to bring it to the desired computation-inducing state. Lower values suggest more flexible materials, resulting in a more efficient hardware-in-the-loop optimization. This investigation has been carried out using only the NM algorithm, keeping all of its parameters the same in every experiment.

The results shown in Table II provide the values of the objective function (2) for various concentrations of SWCNT/PBMA materials for the three different Boolean functions. The table shows a clear transition concentration point (1%) above which the objective function value for all three Boolean functions is zero. Below this point, the objective function's values are greater than zero, showing that solutions for the

TABLE II. Objective function values for various concentrations of SWCNT/PBMA composites for OR, AND, and half adder optimization.

Concentration (wt. %)	OR	AND	Half-adder
0.11	22	6	14
0.25	9	6	17
0.51	6	6	9
0.74	4	3	1
0.99	0	0	0
1.49	0	0	0
2.39	0	0	0

optimization problems have not been found, i.e., the algorithm failed to converge to an optimum.

Figure 9 shows a plot of the number of objective function evaluations performed to reach the solution, with objective function values given in Table II for different nanotube concentrations. In a similar manner to the convergence results, there are two distinct regions; one (above 1% concentration) where the material converges quickly to an optimal solution and a second (below 1%) where the algorithm runs for a long time and practically exhausts the maximum number of iterations allowed. Note that in the NM algorithm the number of function evaluations per iteration is not constant, hence the different number of objective function evaluations at the maximum number of iterations where the algorithm fails to converge.

The AND and the OR gate both show very quick convergence when over the critical concentration threshold percentage, taking fewer than 50 evaluations. The quickest convergence was in fact at the critical percentage of 1%. The number of evaluations required to converge to an optimum increases slightly up to the maximum concentration of 2.39%; this can be attributed to the randomness introduced to the search algorithm.

For the half-adder problem, again there is the critical point at 1% where the number of evaluations drops from over 1700 to around 300. The number of objective function evaluations required for the OR and AND gates when an optimal solution is found, is always less than those required for the half-adder. The reason for that is that the optimization algorithm aims at making two locations on the material behave as two distinct logic gates at the same time, i.e., for the same input. Hence, the increased complexity of the circuit consisting of two gates requires more function evaluations in order to reach an optimal solution. Because the elements of the circuit are two gates, the 1% concentration threshold is retained although the convergence is at different solutions. As can be seen, the effort required by the NM algorithm to find optimum configuration voltage depends almost linearly on the nanotube concentration in the composite film. A denser, randomly dispersed medium is more flexible and is easier to bring to a state where the inputs map

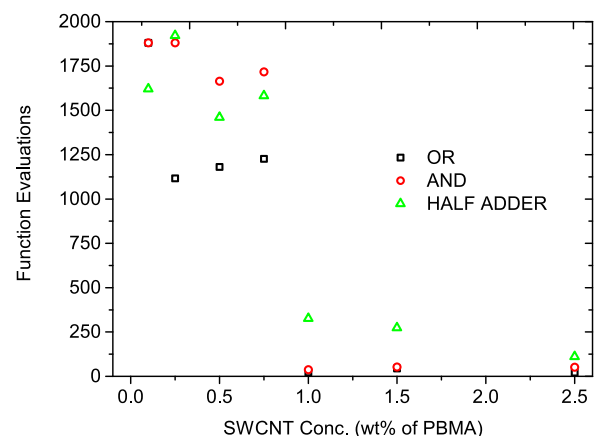


FIG. 9. Number of function evaluations versus SWCNT concentration of SWCNT/PBMA composites for OR, AND and half adder optimization.

correctly to all possible outputs, following the interpretative threshold-logic scheme outlined.

Table III in the Appendix provides the solutions reached by the algorithm. In all cases the number of configuration voltages is five due to the board's design. The functional relationships $f_{j,p}(\mathbf{x})$ of Eq. (4) is $\theta = \beta V_1$ for the standalone AND and OR gates; for the half-adder the carry's threshold is $\theta_{1,1} = \beta V_1$ and the sum's thresholds are $\theta_{2,1} = \beta V_2$ and $\theta_{2,2} = \beta V_3$. This is an arbitrary choice that has yielded good results. For the standalone AND and OR gates an expression $\theta = V_{b_1}$, i.e., the same voltage to denote the logic 1 at the exit as the one used at the input, is feasible. This is still possible even for a more complicated function as reported in Ref. 3.

Table IV in the Appendix provides the material responses in terms of average voltages measured and their standard deviation, when a particular binary pair is given as input for all Boolean functions and material concentrations.

The results shown in Tables III and IV reflect and explain the convergence results reported in Table II. The solutions reached for concentrations 0.11%–0.74%, do not result in the desired behavior. For the standalone OR and AND gates it is clear the material at low concentrations is non-responsive; the recorded values are basically noise from the instrumentation and small positive offsets from small voltage bias. It can also be seen in Table III that for these concentrations, the algorithm terminates at the same solution for the AND gate problem. This is because it responds to the measured objective function values in the same way for the three training sessions, although the material response is different in each case, as can be seen in Table IV. A common feature of the material response of these concentrations is the variance of the measured outputs when binary inputs are sent. The standard deviation in these cases is quite large. Table IV shows that as the concentration increases the responses' variance decreases and it is when the standard deviation is of the order of 8 mV that the optimization problem converges to an optimum solution. The larger the variance, the larger the uncertainty of the actual response is. The cause and effect relationship between the configuration and the measured output voltages, required by the optimization to make sense of out searching the solution space, breaks down.

A final comment on the results shown in Tables III and IV is concerned with the threshold values. In some cases, these are very near the value of a particular material response; however, the responses themselves are quite separated and therefore a different threshold can be used instead of the one determined by the optimization algorithm. It is the end effect of having different and discernible responses that is important and not the threshold values themselves. The fact that the threshold interpretation scheme is included explicitly in the problem formulation directs the optimization to find solutions where the required truth tables are achieved. A simple review of the responses is enough to update the thresholds to more suitable values, always respecting of course the necessary ordering.

These results suggest that for making this type of material behave as a simple computing device, a certain concentration level of conducting elements (SWCNTs) is required. This concentration is related directly to the point at which conductivity starts rapidly increasing, i.e., the percolation threshold of the conductive network within the polymer.

Below this point there are not enough connections within the network to conduct between all nodes in the system.

It should be stressed that in this work optimization is performed on a fixed material system (the conductive filler is not mobile within the polymer matrix). Although the physical structure of the composite will not change during training experiments, the application of electric fields between different electrodes is likely to alter the conductivity throughout the network. This change in conductivity is likely to be the mechanism for optimizing the material system.

IV. CONCLUSIONS

This work has shown that the complex electrical and mechanical nature of SWCNT/PBMA composites can be exploited and used in a form of unconventional computing. The composite thin film shows a change in physical properties at a concentration of SWCNTs of 1.0 wt. %, suggesting that at this point a mechanical percolating threshold is reached. The nature of the SWCNT reinforcement in the composite results in a shear-thinning behavior at high shear rates. This mechanical percolation threshold also corresponds to a change in the electrical conductivity of the material. Above 1.0 wt. %, the rate of increase in conductivity is reduced suggesting that a complete network is already present, linking the two electrodes. At the lower concentrations (0.11%), the network is sparse and in this region the field dependent Poole-Frenkel process provides a good fit to the data.

The SWCNT/PBMA composite has been used for performing a computational task when mounted on a specially designed hardware platform. A threshold behavior with respect to its SWCNT concentration is also observed for its successful configuration for performing Boolean function evaluations. Using a specific interpretation of the measurements collected in conjunction with an optimization algorithm, the material's conductive properties are changed so that the desired behavior is achieved. For the NM algorithm, a threshold of 1 wt. % was observed. This is a similar concentration to the values observed for changes in the mechanical and electrical behavior of the composite. The result indicates a clear link between the physical properties of a material and its ability to perform meaningful computation.

More complex conductive networks, based on liquid host materials may offer increased flexibility, whereas simple systems based on conducting polymers or carbon black may offer similar results for a less complex network. Work is in hand using other material systems and different computational problems to provide further insight into this intriguing interface between computer science and materials science.

ACKNOWLEDGMENTS

The research leading to these results has received funding from the European Community's Seventh Framework Programme (FP7/2007-2013) under grant agreement no. 317662 (NANOscale Engineering for Novel Computation using Evolution—NASCENCE, <http://www.nascence.eu>). We also acknowledge the support from EU FP7 grants: FUNPROB (GA-269169), NanoEmbrace (GA-316751) and the Royal Academy of Engineering/Leverhulme Trust Senior Research Fellowship scheme.

APPENDIX: ADDITIONAL RESULTS

This Appendix contains additional data relating to the computational experiments (Sec III B).

TABLE III. Points (V , in Volts) where the NM algorithm convergences for the OR, AND and half-adder Boolean functions.

Concentration (wt. %)	OR	AND	Half-adder
0.11	$V_1 = 1.117, V_2 = 1.524,$ $V_3 = 1.697, V_4 = 0.289,$ $V_5 = 1.546, V_{b1} = 0.243,$ $\beta = 0.40759, \theta = 0.455$ (Failed to converge)	$V_1 = 0.032, V_2 = 0.481,$ $V_3 = 1.232, V_4 = 1.584,$ $V_5 = 1.111, V_{b1} = 0.186,$ $\beta = 0.25521, \theta = 0.008$	$V_1 = 2.074, V_2 = 0.098,$ $V_3 = 0.865, V_4 = 3.253,$ $V_5 = 2.008, V_{b1} = 2.940,$ $\beta = 1.00000, \theta_{1,1} = 2.074,$ $\theta_{2,1} = 0.098, \theta_{2,2} = 0.865$
0.25	$V_1 = 0.032, V_2 = 0.481,$ $V_3 = 1.232, V_4 = 1.584,$ $V_5 = 1.111, V_{b1} = 0.186,$ $\beta = 0.25521, \theta = 0.008$ (Failed to converge)	$V_1 = 0.032, V_2 = 0.481,$ $V_3 = 1.232, V_4 = 1.584,$ $V_5 = 1.111, V_{b1} = 0.186,$ $\beta = 0.25521, \theta = 0.008$	$V_1 = 2.777, V_2 = 0.365,$ $V_3 = 1.429, V_4 = 0.301,$ $V_5 = 0.642, V_{b1} = 2.643,$ $\beta = 0.53720, \theta_{1,1} = 1.492,$ $\theta_{2,1} = 0.196, \theta_{2,2} = 0.768$
0.51	$V_1 = 0.390, V_2 = 1.335,$ $V_3 = 1.574, V_4 = 2.323,$ $V_5 = 0.000, V_{b1} = 1.096,$ $\beta = 0.05737, \theta = 0.022$ (Failed to converge)	$V_1 = 0.032, V_2 = 0.481,$ $V_3 = 1.232, V_4 = 1.584,$ $V_5 = 1.111, V_{b1} = 0.186,$ $\beta = 0.25521, \theta = 0.008$	$V_1 = 2.028, V_2 = 0.331,$ $V_3 = 2.270, V_4 = 1.672,$ $V_5 = 0.518, V_{b1} = 2.568,$ $\beta = 0.82959, \theta_{1,1} = 1.682,$ $\theta_{2,1} = 0.275, \theta_{2,2} = 1.883$
0.74	$V_1 = 1.574, V_2 = 1.007,$ $V_3 = 0.773, V_4 = 0.401,$ $V_5 = 0.862, V_{b1} = 0.915,$ $\beta = 0.03641, \theta = 0.021$ (Failed to converge)	$V_1 = 0.447, V_2 = 1.891,$ $V_3 = 0.232, V_4 = 0.750,$ $V_5 = 1.137, V_{b1} = 1.893,$ $\beta = 0.64498, \theta = 0.288$	$V_1 = 1.491, V_2 = 0.071,$ $V_3 = 2.394, V_4 = 0.745,$ $V_5 = 1.608, V_{b1} = 1.671,$ $\beta = 0.65274, \theta_{1,1} = 0.973,$ $\theta_{2,1} = 0.046, \theta_{2,2} = 1.563$
0.99	$V_1 = 0.419, V_2 = 0.681,$ $V_3 = 1.663, V_4 = 2.468,$ $V_5 = 1.497, V_{b1} = 0.698,$ $\beta = 0.35765, \theta = 0.150$ (Converge to optimum)	$V_1 = 0.510, V_2 = 0.765,$ $V_3 = 0.612, V_4 = 0.475,$ $V_5 = 1.691, V_{b1} = 0.683,$ $\beta = 0.89508, \theta = 0.456$	$V_1 = 2.272, V_2 = 0.300,$ $V_3 = 2.398, V_4 = 0.666,$ $V_5 = 1.396, V_{b1} = 1.623,$ $\beta = 0.66852, \theta_{1,1} = 1.519$ $\theta_{2,1} = 0.201, \theta_{2,2} = 1.603$
1.49	$V_1 = 0.225, V_2 = 0.902,$ $V_3 = 1.541, V_4 = 0.671,$ $V_5 = 1.181, V_{b1} = 0.833,$ $\beta = 0.61500, \theta = 0.138$ (Converge to optimum)	$V_1 = 1.406, V_2 = 0.906,$ $V_3 = 2.405, V_4 = 1.582,$ $V_5 = 1.535, V_{b1} = 0.833,$ $\beta = 0.64142, \theta = 0.902$	$V_1 = 2.093, V_2 = 0.282,$ $V_3 = 2.061, V_4 = 1.694,$ $V_5 = 0.920, V_{b1} = 1.670,$ $\beta = 0.78589, \theta_{1,1} = 1.645$ $\theta_{2,1} = 0.222, \theta_{2,2} = 1.620$
2.39	$V_1 = 0.313, V_2 = 0.802,$ $V_3 = 0.260, V_4 = 0.218,$ $V_5 = 1.999, V_{b1} = 1.026,$ $\beta = 0.83911, \theta = 0.263$ (Converge to optimum)	$V_1 = 1.217, V_2 = 2.857,$ $V_3 = 2.130, V_4 = 2.420,$ $V_5 = 2.584, V_{b1} = 0.880,$ $\beta = 0.80235, \theta = 0.976$	$V_1 = 1.724, V_2 = 0.407,$ $V_3 = 1.587, V_4 = 1.096,$ $V_5 = 0.595, V_{b1} = 1.819,$ $\beta = 0.87398, \theta_{1,1} = 1.507,$ $\theta_{2,1} = 0.356, \theta_{2,2} = 1.387$

TABLE IV. Material response to binary input pairs for each Boolean function (Volts).

Concentration (wt. %)		Binary inputs				Std. dev	Binary inputs			
		(0,0)	(0,1)	(1,0)	(1,1)		(0,0)	(0,1)	(1,0)	(1,1)
OR gate										
0.11	Mean	-0.105	-0.101	-0.104	-0.115	0.040	0.046	0.039	0.031	
0.25	Mean	-0.515	-0.448	-0.431	-0.511	0.206	0.232	0.226	0.185	
0.51	Mean	-0.007	0.001	-0.002	-0.007	0.015	0.011	0.017	0.013	
0.74	Mean	0.054	0.302	0.070	0.319	0.045	0.054	0.048	0.055	
0.99	mean	0.113	0.481	0.180	0.514	0.007	0.007	0.007	0.008	
1.49	Mean	0.075	0.728	0.166	0.826	0.009	0.008	0.009	0.008	
2.39	Mean	0.098	0.702	0.296	0.890	0.008	0.009	0.009	0.008	
AND gate										
0.11	Mean	-0.121	-0.120	-0.117	-0.127	0.041	0.045	0.042	0.032	
0.25	Mean	-0.466	-0.391	-0.380	-0.478	0.258	0.241	0.258	0.207	

TABLE IV. (Continued.)

		Binary inputs					Binary inputs				
0.51	Mean	-0.006	-0.006	0.000	-0.011	Std. dev	0.019	0.016	0.021	0.011	
0.74	Mean	0.096	0.234	0.101	0.253	Std. dev	0.046	0.049	0.047	0.049	
0.99	Mean	0.109	0.433	0.136	0.466	std. dev	0.031	0.007	0.007	0.008	
1.49	Mean	0.217	0.818	0.261	0.915	Std. dev	0.050	0.009	0.009	0.008	
2.39	Mean	0.526	0.946	0.595	1.129	Std. dev	0.077	0.009	0.009	0.008	
Half-adder circuit											
0.11	Mean (S)	0.671	1.368	0.750	1.514	Std. dev (S)	0.493	0.492	0.508	0.569	
	Mean (C)	0.941	0.961	1.082	1.152	Std. dev (C)	0.679	1.738	0.692	0.783	
0.25	Mean (S)	0.618	0.980	0.807	1.074	Std. dev (S)	0.361	0.435	0.400	0.497	
	Mean (C)	0.658	0.816	0.875	0.880	Std. dev (C)	0.388	0.505	0.457	0.559	
0.51	mean (S)	0.202	1.810	0.426	2.044	Std. dev (S)	0.139	0.124	0.128	0.129	
	Mean (C)	0.913	1.014	0.971	1.285	Std. dev (C)	0.752	0.727	0.750	0.747	
0.74	Mean (S)	0.0334	1.517	0.150	1.638	Std. dev (S)	0.017	0.015	0.018	0.015	
	Mean (C)	0.443	1.094	0.507	1.249	Std. dev (C)	0.262	0.266	0.257	0.274	
0.99	Mean (S)	0.152	1.365	0.403	1.621	Std. dev (S)	0.017	0.013	0.017	0.013	
	Mean (C)	0.321	1.453	0.524	1.668	Std. dev (C)	0.008	0.007	0.008	0.007	
1.49	Mean (S)	0.094	1.452	0.339	1.684	Std. dev (S)	0.018	0.015	0.015	0.016	
	Mean (C)	0.188	1.503	0.381	1.695	std. dev (C)	0.008	0.008	0.008	0.007	
2.39	Mean (s)	0.199	1.359	0.551	1.688	Std. dev (S)	0.017	0.015	0.017	0.008	
	Mean (C)	0.287	1.363	0.622	1.702	Std. dev (C)	0.009	0.007	0.009	0.016	

¹J. Miller, S. Harding, and G. Tufte, "Evolution-in-materio: evolving computation in materials," *Evol. Intell.* **7**, 49–67 (2014).

²H. Broersma, F. Gomez, F. Miller, M. Petty, and G. Tufte, "NASCENCE project: Nanoscale engineering for novel computation using evolution," *Int. J. Unconvent. Comput.* **8**, 313–317 (2012).

³A. Kostialis, M. K. Massey, F. Qaiser, D. A. Zeze, C. Pearson, and M. C. Petty, "Logic gate and circuit training on randomly dispersed carbon nanotubes," *Int. J. Unconvent. Comput.* **10**, 473–497 (2014).

⁴N. G. Sahoo, S. Rana, J. W. Cho, L. Li, and S. H. Chan, "Polymer nanocomposites based on functionalized carbon nanotubes," *Prog. Polym. Sci.* **35**, 837–867 (2010), topical Issue on Nanocomposites.

⁵W. Bauhofer and J. Z. Kovacs, "A review and analysis of electrical percolation in carbon nanotube polymer composites," *Compos. Sci. Technol.* **69**, 1486–1498 (2009), CNT-NET 07 Special Issue with regular papers.

⁶V. Skákalová, U. Dettlaff-Weglikowska, and S. Roth, "Electrical and mechanical properties of nanocomposites of single wall carbon nanotubes with pmma," *Synth. Met.* **152**, 349–352 (2005); Proceedings of the International Conference on Science and Technology of Synthetic Metals.

⁷J. A. Nelder and R. Mead, "A simplex method for function minimization," *Comput. J.* **7**, 308–313 (1965).

⁸C. T. Kelley, *Iterative Methods for Optimization* (Siam, 1999), Vol. 18.

⁹S. Schulz, G. Faiella, S. Buschhorn, L. Prado, M. Giordano, K. Schulte, and W. Bauhofer, "Combined electrical and rheological properties of shear induced multiwall carbon nanotube agglomerates in epoxy suspensions," *Eur. Polym. J.* **47**, 2069–2077 (2011).

¹⁰O. Regev, P. ElKati, J. Loos, and C. Koning, "Preparation of conductive nanotubepolymer composites using latex technology," *Adv. Mater.* **16**, 248–251 (2004).

¹¹A. Ltaief, A. Bouazizi, and J. Davenas, "Charge transport in carbon nanotubes-polymer composite photovoltaic cells," *Materials* **2**, 710–718 (2009).

¹²A. S. Jombert, K. S. Coleman, D. Wood, M. C. Petty, and D. A. Zeze, "Poole-Frenkel conduction in single wall nanotube composite films built up by electrostatic layer-by-layer deposition," *J. Appl. Phys.* **104**, 094503 (2008).

¹³D. J. Perello, W. J. Yu, D. J. Bae, S. J. Chae, M. J. Kim, Y. H. Lee, and M. Yun, "Analysis of hopping conduction in semiconducting and metallic carbon nanotube devices," *J. Appl. Phys.* **105**, 124309 (2009).